Generalized continuum media confronted to long and short wavelength instabilities in architected materials

Christelle Combescure

To cite this version:

Christelle Combescure. Generalized continuum media confronted to long and short wavelength instabilities in architected materials. 2022. ⟨hal-03521030v2⟩

HAL Id: hal-03521030
https://hal.science/hal-03521030v2

Preprint submitted on 27 Jan 2022

Generalized continuum media confronted to long and short wavelength instabilities in architected materials.

Christelle Combescure[1,2*]

[1*]CREC Saint-Cyr, Académie Militaire de Saint-Cyr Coetquidan, F-56380, Guer, France.
[2]IRDL, Univ. Bretagne Sud, UMR CNRS 6027, F-56100, Lorient, France.

Corresponding author(s). E-mail(s):
c.combescure@st-cyr.terre-net.defense.gouv.fr;

Abstract

In the context of architected materials, it has been observed that both long-wavelength instabilities leading possibly to localization and short-wavelength commensurate to cell-size instabilities leading to the apparition of a deformation pattern could occur. This work compares the ability of two families of higher order equivalent media, namely strain-gradient and micromorphic media, to capture both mesoscale cell-commensurate and long-wavelength macroscopic instabilities in those materials. The studied architected material consists in a very simple one-dimensional arrangement of non-linear springs, thus allowing for analytical or nearly analytical treatment of the problem, dismissing any uncertainties or imprecisions coming from a numerical method. A numerical solving of the problem is then used to compare the post-buckling predictiion of both models. The study concludes that, even on a very simple case, it is impossible for a strain-gradient Taylor-series expansion type of homogenization method to capture the cell-commensurate instabilities while the micromorphic medium can capture both instabilities but fails to converge properly in the post-buckling regime when localization appears. Micromorphic media are thus the family of equivalent continuum model that are to prefer when dealing with the possibility of patterning inside a structured medium, but if localization is to consider, it would be interesting to combine both strategies into a micromorphic, gradient enhanced equivalent medium.

1 Introduction

Due to their interesting and sometimes even exotic mechanical properties, architected materials are more and more studied nowadays. As defined in [1–3], architected materials consists in an arrangement of material on at least three length scales : the microscopic scale, describing the constitutive material(s) composition, the macroscopic scale, describing the structure composed by the architectured material and the mesoscopic scale(s) describing the constitutive material(s) arrangement in space (see. Fig.1).

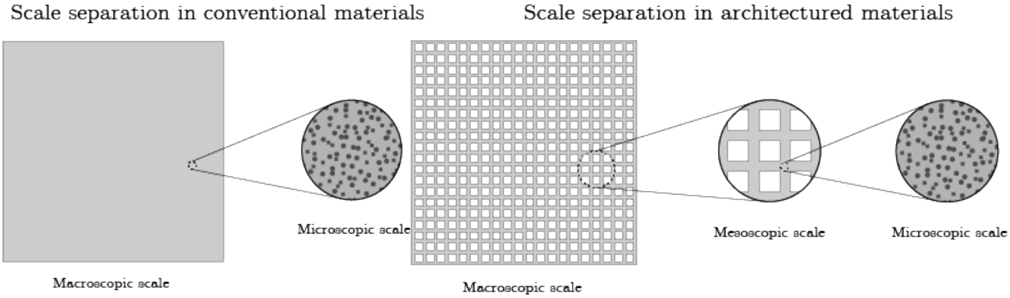

(a) conventional material (b) architected material

Fig. 1: Difference in scale separation in conventional materials and architectured materials. (a) In conventional materials, there are two distinct scales: the macroscopic scale and the microscopic scale, (b) In architectured materials, there are three distinct scales: like in classical materials there are macroscopic and microscopic scales but a third, intermediate "mesoscopic" scale exists of the order of the material's Representative Volume Element size.

The behavior of such materials when submitted to compressive loading has been extensively studied and experiments have led to the conclusion that, when architected materials have a periodic mesoscale arrangement, meaning that they are composed of periodic unit cells, two types of instabilities can occur in those materials : (i) long-wavelength instabilities, that take place at the macroscopic scale and can lead to either global buckling or localization and (ii) short-wavelength "cell-commensurate" instabilities that creates a deformation pattern at the mesoscopic scale. These two types of instabilities are illustrated on Fig.2 alongside with a localized deformation. Localization can happen after a long-wavelength instability and in the case presented in Fig.2.c, a shortwavelength instability appeared first, followed by a long-wavelength instability that lead to a localization as explained in [4].

When dealing with architected materials, it is common to have a scale separation between all scales, meaning that the number of mesoscopic cells in the whole structure can be large. As a consequence, the computation of

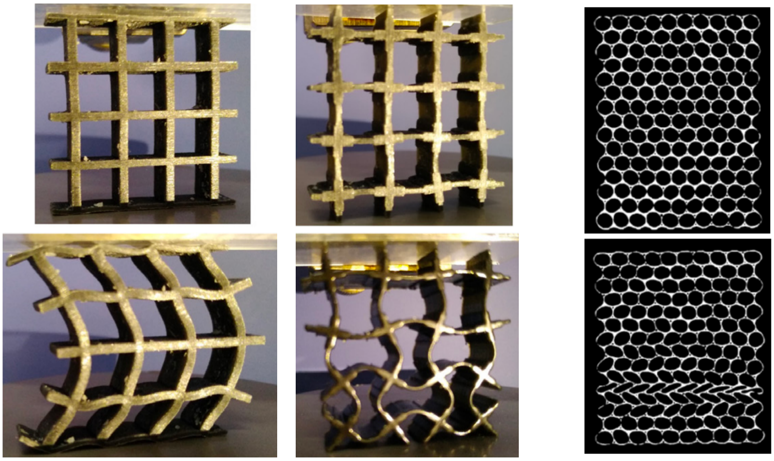

(a) macroscopic buckling (b) mesoscopic buckling (c) localization

Fig. 2: Various types of instabilities observed in architectured materials. (a) and (b) from [5] and (c) from [6]

the non-linear behavior of these structures when submitted to compressive loadings can lead to excessively large amount of time if all the mesoscopic cells have to be taken into account. It is thus quite common to try to build an equivalent continuum medium to the architected material, able to capture its essential behaviors, in order to reduce the computation time. Additionally, in the context of designing the mesoscopic geometry of the unit cell, optimisation procedures based on homogenization and deshomogenization techniques have been proven recently very efficient. Finally, as presented in the coming paragraph, it has been shown that generalized media are to consider if one wants to capture instabilities in architected materials. Before reviewing the scientific literature on the generalized media for short and long-wavelength instabilities, it can be useful to present the two main families of generalized media.

A scheme from [7] and reproduced in Fig.3 presents the two families that stem from a classical Cauchy medium when trying to generalize the kinematics. From the left to the right, rotation then stretch are added to the kinematics. For higher-order continua these extensions are independent DOF, while for higher-grade continua they are controlled by higher-order gradients of the displacement field. For the sake of simplicity, in the remainder of this article, higher-order media will be referred to as ”micromorphic” media whereas higher-grade will be named ”strain-gradient”.

In the context of instabilities appearing in periodic architected materials, pioneer article by [8] studied the ability of a strain-gradient model to capture long wavelength instabilities and localization appearing in a periodic arrangement of one-dimensional springs. This model, built by a Taylor expansion

$$\begin{tikzcd}
 & \textit{Rotation}: & \textit{Stretch}: \\
 & \text{Cosserat} \arrow[r] \arrow[dd, "\simeq"] & \text{Micromorphic} \arrow[dd, "\simeq"] \\
\text{Classical continua} \arrow[ur, "Higher-order"] \arrow[dr, "Higher-grade"'] & & \\
 & \text{Koiter} \arrow[r] & \text{Strain-Gradient}
\end{tikzcd}$$

Fig. 3: Basic extensions of a classical continuum. From [7].

of the mesoscopic displacement, appeared to be perfectly able to capture the macroscopic long-wavelength instability and the subsequent localization phenomenon that appeared. No mention of the possible short-wavelength buckling was made in this article. In [9], authors propose a quasi-continuum model based also on strain-gradient in order to capture both long and short wavelength instabilities appearing in a periodic arrangement of atoms linked by non-linear interatomic potentials. The conclusion is that the quasi-continuum media can capture some sort of short-wavelength instability but it appears that the buckling threshold is not appropriately captured by the model. Finally, attention on short wavelength instabilities has recently grown, because of their possible application for creating band gaps when propagating elastic waves. [10] have recently proposed a micromorphic computational homogenization procedure to capture patterning, meaning short-wavelength instabilities.

Based on the observation that, in architected materials, both short and long-wavelength instabilities can occur, and that both micromorphic and strain-gradient media have been proposed in the litterature to capture such behaviors, it is of interest in this study to compare the ability of these two types of generalized media to capture each type of instability on a very simple problem. As a consequence, the example of a periodic arrangement of non-linear springs, as presented in Fig.4 below has been proposed.

2 Discrete system

2.1 Setting

Consider a one-dimensional structure composed of initially equally spaced nodes connected by non-linear elastic springs, campled at one end and submitted to an end displacement or force at the other end. The node spacing is denoted by b and the total length of the structure is $L = Nb$ where $N >> 1$. The structure thus has a total number of $N + 1$ nodes. A typical node n is connected to its adjacent nodes m with possibility to connect to nodes further than the immediate neighboring node as displayed in Fig.4 where a connection

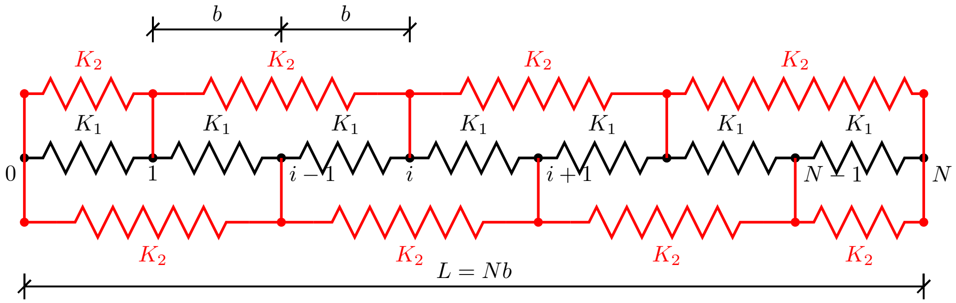

Fig. 4: 1D arrangement of non-linear springs with connection to next-to-neighbour node, displaying both cell-commensurate and long-wavelength instabilities. Black and red springs have different internal energies represented by the letter K indexed by a number.

to the next-to-neighbor node is presented. As such, an integer q indicates the maximum number of neighboring nodes to which each node is connected on each side. The strain ϵ_p in a spring of length pb $(1 \leq p \leq q)$ attached to node n is given by Equation 1:

$$\epsilon_n^{p+} = \frac{u_{n+p} - u_n}{pb} \quad \text{or} \quad \epsilon_n^{p-} = \frac{u_n - u_{n-p}}{pb}. \tag{1}$$

The stored energy density in a spring of length pb is $w_p(\epsilon^p)$. The stored energy density of the discrete structure, denoted W, equals half of the energy of all springs connected to an interior node n divided by nodal spacing b, as presented in Equation 2:

$$W = \frac{1}{2b} \sum_{n=0}^{n=N} \sum_{p=1}^{q} p \left[w_p(\epsilon_p^{n+}) + w_p(\epsilon_p^{n-}) \right]. \tag{2}$$

The total energy of the system is then defined by:

$$\mathcal{E} = W - \frac{1}{Nb} F u_N, \tag{3}$$

where F is the force exerted at the end node N necessary to induce the displacement u_N.

The discrete system is considered to be at equilibrium when the derivative of this energy with respect to the displacement of node n is null for all nodes n inside the system. This condition give rises to the following system of difference equation :

$$\frac{\partial W}{\partial u_n} = 0 \quad \forall n \in [0, N-1] \qquad ; \qquad \frac{\partial W}{\partial u_N} = \frac{F}{Nb}. \tag{4}$$

A solution of the system of equilibrium equations Equation 4 is called an equilibrium state and noted $\overset{r}{u}$. In order to access stability of this equilibrium state, perturbations δu_n are introduced and the positive definiteness of the quadratic part of the energy expansion is studied:

$$\left.\frac{\partial^2 W}{\partial u_n \partial u_m}\right|_{\overset{r}{u}} \delta u_m > 0? \tag{5}$$

The system is said to be stable whenever Equation 5 is true and unstable otherwise.

Following recommendations of [9], we will study, in this paper, only the case $q = 2$ depicted in Fig.4. As for the non-linear stored energy per unit length for one spring, it will be taken equal to the one proposed in the Type A model of [8]:

$$w_p(\epsilon) = \frac{1}{2} K_p \epsilon^2 - \frac{1}{4} M_p \epsilon^4 + \frac{1}{6} N_p \epsilon^6, \tag{6}$$

where K_p, M_p and N_p are *stiffness*-like coefficients for the spring and are then considered to be positive intrinsic constants. One recognizes, in the quadratic term, the usual stored energy function for linear springs $w_p(\epsilon) = \frac{1}{2} K_p \epsilon^2$. Thus K_p has to be positive in order to ensure realistic springs.

2.2 Stability Analysis

The discrete system, in the case $q = 2$ and using the stored energy function presented in Equation 6, presents an equilibrium equation for a given inner node n of the form:

$$\begin{aligned} 0 = b^4 K_1 \left((u_n - u_{n+1}) - (u_{n-1} - u_n)\right) &- b^2 M_1 \left((u_n - u_{n+1})^3 - (u_{n-1} - u_n)^3\right) \\ &+ N_1 \left((u_n - u_{n+1})^5 - (u_{n-1} - u_n)^5\right) \\ + \frac{1}{32} \Big[16 b^4 K_2 \left((u_n - u_{n+2}) - (u_{n-2} - u_n)\right) &- 4 b^2 M_2 \left((u_n - u_{n+2})^3 - (u_{n-2} - u_n)^3\right) \\ &+ N_2 \left((u_n - u_{n+2})^5 - (u_{n-2} - u_n)^5\right) \Big] . \end{aligned} \tag{7}$$

A trivial solution to this equation is given by $u_n = u_{n+p} \quad \forall n \in [0, N] \ \forall -q \leq p \leq q$, leading to a uniform displacement of all the nodes corresponding to a global translation that is of no interest for this study.

Another solution would be $u_n - u_{n+1} = u_{n-1} - u_n$ & $u_n - u_{n+2} = u_{n-2} - u_n \quad \forall n \in [0, N]$ which corresponds to uniform strain $\epsilon_p^{n+} = \epsilon_p^{n-} = \overset{0}{\epsilon} \quad \forall n \in [0, N] \quad \forall -q \leq p \leq q$ of the discrete system. This solution will be named *principal solution* and further noted $\overset{0}{u}$. Of interest in this study will be the stability of this principal solution $\overset{0}{u}$.

Following the methodology proposed in [4, 11, 12], we will use the Bloch-waves (also termed the phonon or Floquet method) to study stability of the principal solution. This method consists in perturbing the studied solution by plane-waves such that the perturbation of node $n+p$ is related to the perturbation of node n by Equation 8:

$$\delta u_{n+p} = \delta u_n(k) e^{2i\pi kpb}, \tag{8}$$

where k is the normalized spatial wavenumber corresponding to the imposed plane-wave.

Given that $q = 2$, the only non-zero terms in the quadratic part of the energy expansion $\left.\frac{\partial^2 W}{\partial u_n \partial u_m}\right|_{\overset{0}{u}} \delta u_m$ are defined by $n - q \leq m \leq n + q$. For the sake of simplicity, these terms will be noted $C_{n,m} = \left.\frac{\partial^2 W}{\partial u_n \partial u_m}\right|_{\overset{0}{u}}$ and can be directly computed as:

$$\begin{gathered}
C_{n,n} = \tfrac{1}{b^2}\left[2(K_1 - 3M_1\overset{0}{\epsilon}{}^2 + 5N_1\overset{0}{\epsilon}{}^4) + K_2 - 3M_2\overset{0}{\epsilon}{}^2 + 5N_2\overset{0}{\epsilon}{}^4\right] \\
C_{n,n-1} = \tfrac{-1}{b^2}(K_1 - 3M_1\overset{0}{\epsilon}{}^2 + 5N_1\overset{0}{\epsilon}{}^4) = C_{n,n+1} \\
C_{n,n-2} = \tfrac{-1}{2b^2}(K_2 - 3M_2\overset{0}{\epsilon}{}^2 + 5N_2\overset{0}{\epsilon}{}^4) = C_{n,n+2}.
\end{gathered} \tag{9}$$

We are then left with determining the conditions for Equation 10 to be satisfied, in order to ensure stability of the principal solution.

$$C_{n,n-2}e^{-4i\pi kb} + C_{n,n+2}e^{4i\pi kb} + C_{n,n-1}e^{-2i\pi kb} + C_{n,n+1}e^{2i\pi kb} + C_{n,n} > 0. \tag{10}$$

Using expressions for $C_{n,m}$ terms defined in Equation 9 and semi-angle formulæ, Equation 10 simplifies to:

$$\begin{gathered}
\sin^2(\pi kb)\left[K_1 - 3M_1\overset{0}{\epsilon}{}^2 + 5N_1\overset{0}{\epsilon}{}^4 + (1+\cos(2\pi kb))(K_2 - 3M_2\overset{0}{\epsilon}{}^2 + 5N_2\overset{0}{\epsilon}{}^4)\right] > 0 \\
\Leftrightarrow \sin^2(\pi kb)\left[g_1(\overset{0}{\epsilon}) + (1+\cos(2\pi kb))g_2(\overset{0}{\epsilon})\right] > 0,
\end{gathered} \tag{11}$$

where g_1 and g_2 functions, defined as $g_i(\epsilon) = K_i - 3M_i\epsilon^2 + 5N_i\epsilon^4 \;\; i = 1,2$, have been introduced to further simplify the expressions.
This latter expression resembles the one presented in Equation 7 of [9] as it presents a quadratic term of sin.

By studying stability condition presented in Equation 11, it appears that the only unstable wavelengths are:

- the short-wavelength instability associated with wavelength $k = \frac{1}{2b}$ corresponding to a periodic instability at the scale of two springs of length b.

This instability will appear at global strain $\overset{0}{\epsilon}$ solution of $g_1(\overset{0}{\epsilon}) = 0$[1]. This instability was nammed "commensurate" in [9] ;

- the long-wavelength instability corresponding to the case of $k \to 0$ (acoustic branch) appearing when the global strain $\overset{0}{\epsilon}$ is such that $g_1(\overset{0}{\epsilon}) + 2g_2(\overset{0}{\epsilon}) = 0$.

There is then three possible stability regimes depending on the respective values of the stiffness parameters. The conditions for these regimes to appear are presented below. They depend on four conditions. The negation of a condition will be noted with an overline, for instance cond $0 : K_1 > 0 \Rightarrow \overline{\text{cond } 0} : K_1 \leq 0$.

- conditions for a stable path for all imposed global strains:

$$\underbrace{M_1 < \frac{2}{3}\sqrt{5K_1N_1}}_{\text{cond 1}} \quad \& \quad \underbrace{M_2 < \frac{-M_1}{2} + \frac{\sqrt{5}}{3}\sqrt{(K_1+2K_2)(N_1+2N_2)}}_{\text{cond 2}}$$

  For instance, choosing $K_1 = K_2 = N_1 = N_2 = 1$, cond 1 imposes $M_1 < \frac{2\sqrt{5}}{3} \approx 1.49$. Picking $M_1 = 1$, cond 2 leads to $M_2 < \frac{-1}{2} + \sqrt{5} \approx 1.736$, for example $M_2 = 1.6$. The loading path corresponding to this choice of stiffness parameters is plotted in plain blue line in Figure 5.
- conditions for a short-wavelength instability to appear first:

$$\underbrace{M_1 \geq \frac{2}{3}\sqrt{5K_1N_1}}_{\overline{\text{cond 1}}} \quad \& \quad \underbrace{6M_2 + \frac{|K_2N_1 - K_1N_2|}{K_1N_1}\sqrt{9M_1^2 - 20K_1N_1} < 3M_1\left(\frac{K_2}{K_1} + \frac{N_2}{N_1}\right)}_{\text{cond 3}}$$

  For instance, choosing $K_1 = K_2 = N_1 = N_2 = 1$, $\overline{\text{cond 1}}$ implies $M_1 > \frac{2\sqrt{5}}{3} \approx 1.49$. Picking $M_1 = 2$, cond 3 leads to $M_2 < M_1 = 2$; for example $M_2 = 1$. The loading path corresponding to this choice of stiffness parameters is plotted in plain orange line in Figure 5.
- conditions for a long-wavelength instability appearing first along the principal path:

$$\underbrace{M_1 \leq \frac{2}{3}\left(K_2N_1 + K_1(N_1+N_2)\right)\sqrt{\frac{5}{(K_1+2K_2)(N_1+2N_2)}}}_{\text{cond 4}} \quad \& \quad \overline{\text{cond 2}}$$

$$\text{or}$$

$$\overline{\text{cond 4}} \;\&\; \overline{\text{cond 3}}$$

  For instance, choosing $K_1 = K_2 = N_1 = N_2 = 1$, cond 4 implies $M_1 \leq \frac{2\sqrt{5}}{3} \approx 1.49$. Picking $M_1 = -1$, $\overline{\text{cond 2}}$ leads to $M_2 \geq \frac{-1}{2} + \sqrt{5} \approx 2.736$; for

---

[1] corresponding to $\overset{0}{\epsilon}^2 = \frac{3M_1}{10N_1} \pm \frac{1}{10}\sqrt{\frac{9M_1^2 - 20K_1N_1}{N_1^2}}$ with $K_1 < \frac{9M_1^2}{20N_1}$

example $M_2 = 3$. The loading path corresponding to this choice of stiffness parameters is plotted in plain green line in Figure 5.

Additionally, the two previously described instabilities can appear simultaneously whenever $g_1(\overset{0}{\epsilon}) = g_2(\overset{0}{\epsilon})$.

In order to be realistic, the structure has to be stable under null applied strain for all wavelength thus leading to the conditions $K_1 + 2K_2 > 0$ & $K_1 > 0$ which are both automatically satisfied when K_1 and K_2 are taken to be positive, as requested in the problem setting section.

Using g_1 and g_2, a stability diagram can be established in the plane of these two "parameters". Then, since these parameters are actually functions that depends on the global applied strain ϵ, the loading path followed by these functions as ϵ evolves can be plotted. On Figure 5, the stable region is represented in blue with orange and green borders corresponding to short and long-wavelength instability criteria, respectively. This graph also presents examples of loading paths leading to long-wavelength instability (green), short-wavelength instability (orange) or no instability (blue). All these path start in the stable region and evolve to cross either the orange or the green border. If no border is crossed, the path remains stable. The parameters chosen for these paths make them cross the border twice so that they recover stability after a trip in the unstable regime[2] ; this feature is not compulsory and it is possible to design systems that would remain unstable all along.

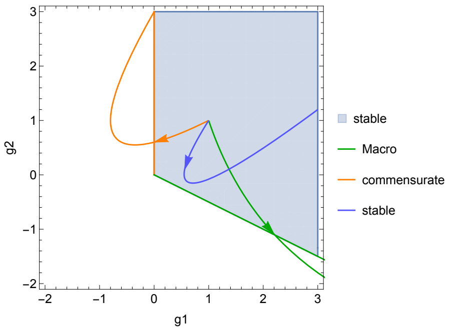

Fig. 5: Stability diagram for the discrete model with $q = 2$. Region of stability is shown in blue. Orange and green borders to this blue stability region correspond to criteria for short and long-wavelength instabilities, respectively. In plain colored lines with arrows are plotted examples of loading paths leading to long-wavelength instability (green), short-wavelength instability (orange) and no instability (blue). Parameters for these paths are stated in the text.

---

[2] The return of stability appears for the green path out of the bounds of the graph that has been zoomed on the zone of interest

3 Homogenization

Of interest in this study is the comparison of the micromorphic-type and the strain-gradient-type homogenization strategies in their ability to capture short and long-wavelength instabilities of non-linear spring assemblies. This section details the derivation of both equivalent continuum energies.

3.1 Strain-gradient equivalent medium

This part follows the strain-gradient energy derivation proposed in [8].

The strain-gradient homogenization strategy is based on a Taylor series expansion of the displacement continuous function $u(x)$ that is assumed to coincide with all equilibrium discrete displacements u_n at nodal points $x_n = nb$ corresponding to node n. As such, using Equation 1, the strains ϵ_n^{p+} and ϵ_n^{p-} in all the non-linear springs affecting node n equilibrium can be expressed as in Equation 12 where the following simplified notation is used $u_{,x} = \frac{du(x)}{dx}$:

$$\begin{aligned} \epsilon_n^{p+} &= \tfrac{u_{n+p}-u_n}{pb} = u_{,x} + \tfrac{1}{2}pbu_{,xx} + \tfrac{1}{6}(pb)^2 u_{,xxx} + \ldots \\ \epsilon_n^{p-} &= \tfrac{u_n-u_{n-p}}{pb} = u_{,x} - \tfrac{1}{2}pbu_{,xx} + \tfrac{1}{6}(pb)^2 u_{,xxx} - \ldots \end{aligned} \tag{12}$$

Introducing this decomposition into the stored energy density of the discrete structure Equation 2 , one gets the following expression for the strain-gradient stored energy, where the discrete sum is naturally replaced by an integral over the length $L = Nb$ of the system:

$$W^s(u_{,x}) = \int_0^L w_1(u_{,x}) + 2w_2(u_{,x}) - \frac{b^2}{24}\left[\left(w"_1(u_{,x}) + 8w"_2(u_{,x})\right)(u_{,xx})^2\right] + O(b^4)dx \tag{13}$$

Thus, using the Type A stored energy function Equation 6, the homogenized strain-gradient macroscopic energy density is then:

$$\begin{aligned} W^s(E) = \int_0^L & \underbrace{E^2\frac{K_1+2K_2}{2} - E^4\frac{M_1+2M_2}{4} + E^6\frac{N_1+2N_2}{6}}_{\mathcal{E}(E)} \\ & + (\nabla E)^2\frac{b^2}{2}\underbrace{\frac{1}{12}\left[-(K_1+8K_2) + 3(M_1+8M_2)E^2 - 5(N_1+8N_2)E^4\right]}_{h(E)} dx. \end{aligned} \tag{14}$$

The equilibrium equation corresponding to this stored energy is found by extremizing it over all admissible displacements δu: $W_{,u}\,\delta u = 0$. This leads, using Euler-Lagrange equations, to Equation 15:

$$\mathcal{E}'(E) - b^2\left(\Delta E\ h(E) + \frac{(\nabla E)^2}{2} h'(E)\right) = F, \tag{15}$$

where F is the external applied force exerted at the end of the structure. A trivial solution to this equation is $E = \overset{0}{E}$ where $\overset{0}{E}$ is a constant. This corresponds to the principal path of our discrete problem.

In order to study the stability of this principal equilibrium state, one must examine the positive definiteness of the second Frechet derivative of the homogenized strain-gradient macroscopic energy regarding all admissible displacement δu and evaluated along the principal path:

$$(W^s{,_{uu}}(\overset{0}{u}, \Delta)\delta u)\delta u = \mathcal{E}"(\overset{0}{E})(\delta u{,_x})^2 - b^2 h(\overset{0}{E}(\delta u{,_{xx}})^2. \tag{16}$$

On can use, without loss of generality, the following admissible functions satisfying the admissible to zero boundary conditions $\delta u(0) = \delta u(L) = 0$:

$$\delta u(x) = \sqrt{\frac{2}{L}} \sum_{k=1}^{\infty} \delta u_n \sin\left(\frac{k\pi x}{L}\right). \tag{17}$$

This yields the stability condition:

$$\sum_{k=1}^{\infty}\left[\mathcal{E}"(\overset{0}{E}) + b^2\left(\frac{k\pi}{L}\right)^2 h(\overset{0}{E})\right]\left(\frac{n\pi}{L}\delta u\right)^2 > 0. \tag{18}$$

As explained in [8], this stability condition is satisfied as long as $\mathcal{E}"(\overset{0}{E}) + b^2\left(\frac{k\pi}{L}\right)^2 h(\overset{0}{E}) > 0$. Using the Type A stored energy function Equation 6, and noting $\ell = \frac{b}{L}$ the non-dimensional length appearing in this problem, the stability condition takes the following form:

$$\begin{aligned}(K_1 + 2K_2) - 3(M_1 + 2M_2)E^2 + 5(N_1 + 2N_2)E^4)\\ + \frac{(\ell k\pi)^2}{12}\left[-(K_1 + 8K_2) + 3(M_1 + 8M_2)E^2 - 5(N_1 + 8N_2)E^4\right] > 0\end{aligned} \tag{19}$$

Critical points correspond to Equation 19 equal to zero, they will thus depend on the value of non-dimensional length parameter ℓ and integer k. The first condition arising when studying instability corresponds to the long-wavelength condition: $\underbrace{K_1 - 3M_1E^2 + 5N_1E^4 + 2(K_2 - 3M_2E^2 + 5N_2E^4)}_{g_1(E)+2g_2(E)} = 0$, second condition corresponds to $k = -\frac{\sqrt{3}}{\ell\pi}$ & $\underbrace{K_1 - 3E^2M_1 + 5E^4N_1}_{g_1(E)} = 0$. But k has to be an integer and ℓ is fixed by the ratio of microscopic to macroscopic lengths. As a consequence, there is little to no chance for this second condition to be respected and thus, the short-wavelength instability will be miscaptured by the strain-gradient equivalent continuum.

3.2 Micromorphic Equivalent medium

The stability analysis of the discrete system has shown that only two unstable modes could occur in the case $q = 2$: a short-wavelength period-doubling instability and a long-wavelength instability. It is of interest in this study to derive *homogenized* models that would be able to capture both modes. The studied system being periodic of period b, the micromorphic homogenization strategy consists in writing the springs node displacements according to the Cauchy-Born hypothesis [13], corresponding to the description of the displacement field as the sum of a homogeneous displacement Ex and a periodic displacement, named *shift*, s:

$$u(x) = Ex + s(x), \tag{20}$$

where E is the applied macroscopic strain supposed to be known, x is the position of the node and $s(x)$ the periodic shift (unknown), function of the node position. This hypothesis is similar to the one usually applied in the periodic homogenization process.

Given that the stability analysis of the discrete system uncovered the possibility for a period-doubling instability to occur, the homogenization will take place on a unit-cell comprising two adjacent nodes n and $n+1$, thus working on a total length of two periods: $2b$. In order to prevent uniform translations, node n is considered to be fixed: $u_n = 0$. With these assumptions, the strains of each spring connected to the studied nodes n and $n+1$ can be computed from Equation 1:

$$\epsilon_n^{1+} = E + \frac{s}{b} \quad ; \quad \epsilon_n^{1-} = \epsilon_{n+1}^{1+} = E - \frac{s}{b} \quad ; \quad \epsilon_n^{2+} = \epsilon_n^{2-} = \epsilon_{n+1}^{2+} = \epsilon_{n+1}^{2-} = E \quad . \tag{21}$$

Using the Type A stored energy function Equation 6 along with the strain expressions derived in Equation 21 and injecting those into the stored energy of the structure composed of 2 nodes (N=1) Equation 2 leads to the following homogenized internal energy:

$$\begin{aligned} W^m(E,s) = \int_0^L & E^2\frac{K_1+2K_2}{2} - E^4\frac{M_1+2M_2}{4} + E^6\frac{N_1+2N_2}{6} \\ & + \frac{K_1-3E^2M_1+5E^4N_1}{2}\left(\frac{s}{b}\right)^2 - \frac{M_1-10E^2N_1}{4}\left(\frac{s}{b}\right)^4 + \frac{N_1}{6}\left(\frac{s}{b}\right)^6 dx \end{aligned} \tag{22}$$

The attentive reader could notice in this last expression that the term gathered in $\mathcal{E}(E)$ – the first order term – is equal to the homogenized internal shift energy Equation 22 when the shift is null $W^s(E,0)$. Additionally, the displacement shift s appears to be always associated with microscopic length b as $\frac{s}{b}$; this term can be called the "deformation shift" and examples later on will explain its physical interpretation. The homogenized internal energy Equation 22 now depends on two state variables: the macroscopic applied strain E and the deformation shift $\frac{s}{b}$. On the one hand, differentiating this internal energy with respect to the macroscopic strain E gives rises to the macroscopic equilibrium of the structure where a loading term F corresponding to the external applied force exerted at the end of the structure appears (Equation 23):

$$\begin{aligned} &E\left(K_1 + 2K_2 - E^2(M_1 + 2M_2) + E^4(N_1 + 2N_2)\right) \\ &+(-3M_1 + 10N_1E^2)E\left(\frac{s}{b}\right)^2 + 5N_1E\left(\frac{s}{b}\right)^4 = F \end{aligned} \tag{23}$$

On the other hand, differentiating this energy with respect to the deformation shift leads to the equation for the internal equilibrium of the periodic unit cell:

$$s\left[b^4\left(K_1 - 3E^2M_1 + 5E^4N_1\right) - b^2\left(M_1 - 10E^2N_1\right)s^2 + N_1s^4\right] = 0\ , \tag{24}$$

which admits several solutions. The trivial solution $s = 0$ describes an homogeneous strain of the structure and corresponds to the principal path. Equation 24 corresponds to the evolution law of state variable deformation shift $\frac{s}{b}$ with respect to macroscopic deformation E.

The stability of the principal path can be studied by looking at the positive definiteness of the matrix defined by the second derivatives of the homogenized total energy with respect to both state variables, evaluated along the principal path (meaning that $s = 0$):

$$\left.\begin{bmatrix} \frac{\partial^2 W^m}{\partial E^2} & \frac{\partial^2 W^m}{\partial E \partial s} \\ \frac{\partial^2 W^m}{\partial E \partial s} & \frac{\partial^2 W^m}{\partial s^2} \end{bmatrix}\right|_{s=0} .$$

When the determinant of this matrix becomes null, the stability of the system is lost. This loss of stability happens if one of the two conditions listed in Equation 25 are satisfied:

$$\underbrace{K_1 - 3M_1E^2 + 5N_1E^4}_{g_1(E)} = 0 \text{ or } \underbrace{K_1 - 3M_1E^2 + 5N_1E^4 + 2(K_2 - 3M_2E^2 + 5N_2E^4)}_{g_1(E)+2g_2(E)} = 0 \tag{25}$$

One can then recognize immediately in these equations the two conditions $g_1(\epsilon) = 0$ and $g_1(\epsilon) + 2g_2(\epsilon) = 0$ established in subsection 2.2.

As a consequence, the homogenized model using the deformation shift as additional state variable has the ability to capture both short-wavelength and long-wavelength instabilities.

4 Numerical study

Strain-gradient models have an internal length, and as such have been proven to be numerically efficient to capture localization phenomena as underlined in [8]. It is thus of interest to compare the numerical efficiency of both models in cases where short-wavelength instabilities appear but also in a case with a long-wavelength instability followed by a localization. These two cases are presented below, they correspond to the orange and green cases presented in the discrete analysis section and are related to the following set of parameters: $K_1 = K_2 = N_2 = N_2 = 1$ and $M_1 = 2$, $M_2 = 1$ for the short wavelength instability and $M_1 = 1$, $M_2 = 2$ for the long wavelength instabiilty. They will be compared with a computation made on the full discrete system including all the springs. The computations have been carried out using a custom home-made bifurcation and branch-following software [14, 15] for the discrete and micromorphic models and using software AUTO-07p [16] for the strain-gradient model.
The problem of interest for this numerical study is an arrangement of 40 springs connecting direct neighboring nodes associated with internal energy $w_1(\epsilon^1)$ and 39 springs connecting next-to neighbor springs associated with internal energy $w_2(\epsilon^2)$. In order to ensure a regular constant strain principal solution, the boundary next-to neighbor springs are in fact connected to their direct neighbor and associated with an internal energy $w_2(\epsilon^1)$ as represented in Figure 4. This arrangement of springs is considered to be clamped on the left end and submitted to an end force F associated with end displacement Δ at the other end.

When using the micromorphic equivalent medium, and internal length has to be set corresponding to the ratio between the microscopic to the macroscopic length. In this model, it has been chosen as $\ell = 1/40$ in accordance with the number of springs in the discrete model. A finite difference scheme has been employed with 40 elements. This number of elements could be increased or decreased without changing the displayed results.

4.1 Short-wavelength instability

Internal energy model parameter are chosen to be $K_1 = K_2 = N_2 = N_2 = 1$ and $M_1 = 2$, $M_2 = 1$ so that the system should display a short-wavelength instability that spans over two nodes, as explained in the discrete analysis section.
Results corresponding to the numerical computation of the problem on the

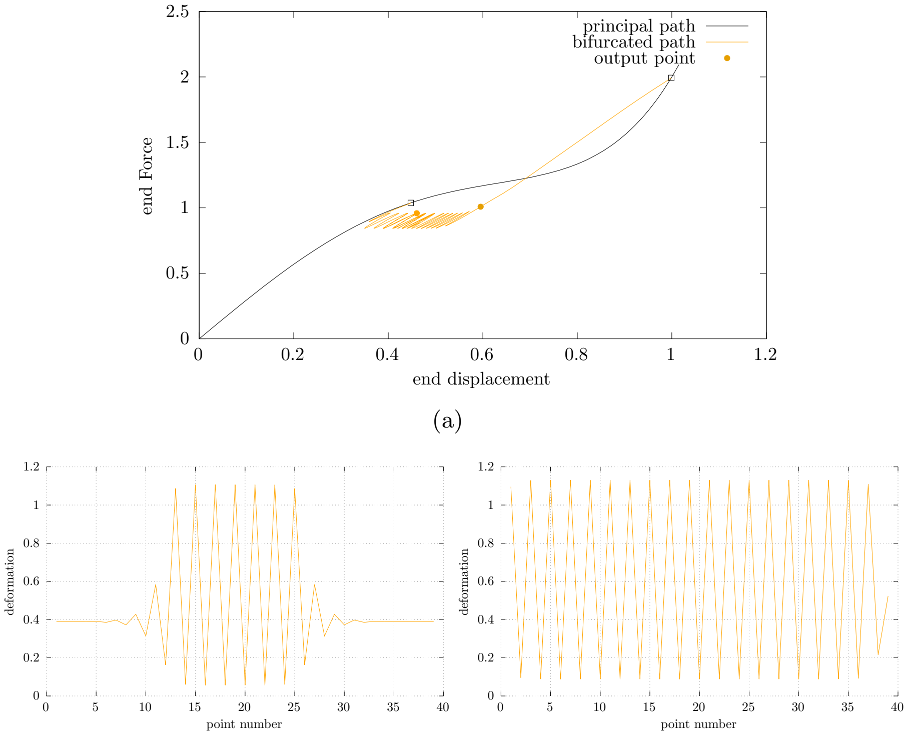

(a)

(b) output point 1

(c) output point 2

Fig. 6: Numerical results of computation on the discrete system. (a) End force-displacement graph with principal path in black and first bifurcated branch in orange. Empty squares mark the location of bifurcation points and the plain circles are the computation points for which bifurcated modes are outputted. (b) first and (c) second bifurcation modes represented in terms of deformation corresponding to the plain circle output points.

discrete system are displayed in Figure 6. The systems shows a monotonic principal branch (Figure 6a) in plain black line with a bifurcation point appearing at $(\Delta_\epsilon, F) = (0.44773, 1.03815)$. From that point, a bifurcated branch in plain orange line emerges that displays wide oscillations corresponding to propagation of the alternate mode across the springs (Figure 6b) to finally reach the entire length of the system Figure 6c. The predicted short-wavelength instability is thus confirmed and appropriately spreads across two nodes as represented by the alternate values of deformation on each node. The systems has a discrepancy in terms of deformation, which loses uniformity near the end, corresponding to the fact that it is not infinite.

When using the micromorphic equivalent medium, the principal path is appropriately captured and the bifurcation point corresponds to $(\Delta_E, F) =$

$(0.447214, 1.0375355)$ with relative error of 10^{-3} on the displacement and of 6.10^{-4} on the force value. No oscillations are present on the bifurcated branch which directly corresponds to a uniform internal shift across the system's length. Figure 7a presents the end force-displacement curve for the micromorphic equivalent medium. In transparent plain orange line is displayed the results on the discrete model for comparison. A very good agreement between the discrete and the micromorphic model can be observed on this curve. This agreement can also be observed when comparing the values of deformation and deformation shift ($= s/b$) coming from the micromorphic medium to the values of the local deformation from the discrete model. Indeed, the micromorphic deformation E corresponds to the mean deformation of the bifurcated mode while the micromorphic deformation shift s/b is the amplitude of the discrete mode oscillations.
Now, when using the strain-gradient equivalent medium, the principal path is also appropriately captured. Several bifurcation points appear on this branch including one before the bifurcation point of interest. The closest bifurcation point to the one found by the discrete model appears at $(\Delta_E, F) = (0.449357, 1.0400949)$ with relative error of 3.10^{-3} on the displacement and of $1.8.10^{-3}$ on the force value, meaning that the error this three times higher than for the micromorphic medium. Additionally, the bifurcated branch differs from the discrete bifurcated branch and does not converge all the way.

From this first numerical study of a short-wavelength bifurcating system, it appears that the micromorphic medium is more precise to capture the onset of short-wavelength bifurcation and more accurate in the prediction of the bifurcated branch than the strain-gradient medium which cannot converge all the way along the bifurcated branch. This confirms the conclusions drawn after the analytical analysis carried out in the homogenization section.

4.2 Long-wavelength instability and localization

Internal energy model parameter are chosen to be $K_1 = K_2 = N_2 = N_2 = 1$ and $M_1 = -1$, $M_2 = 3$ so that the system should display a long-wavelength instability followed by a localization, as explained in the discrete analysis section.

Results corresponding to the numerical computation of the problem on the discrete system are displayed in Figure 8. The systems shows a non-monotonic up-down-up principal branch (Figure 8a) in plain black line which comes to a limit point at $(\Delta_\epsilon, F) = (0.525731, 0.9711368291)$. According to [8], the up-down-up behavior ensures a localization phenomenon appearing after the first turning point. A series of very close bifurcation points appear indeed right after the turning point. The first bifurcation point corresponds to $(\Delta_\epsilon, F) = (0.525852, 0.9711376579)$. From that point, a bifurcated branch in plain green line emerges that an almost horizontal line (called the Maxwell line [17]). This branch actually contains oscillations (see the zoom in Figure 8b corresponding to propagation of the localized mode across the springs (Figure 8d) to finally

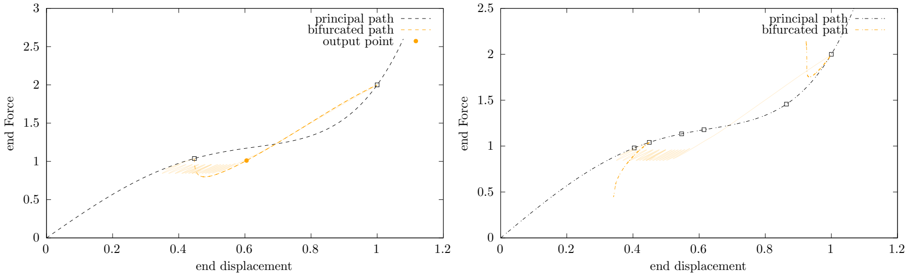

(a) micromorphic medium

(b) strain-gradient medium

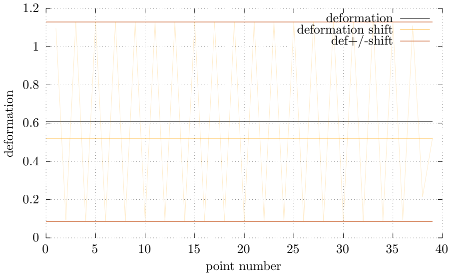

(c) micromorphic deformation mode

Fig. 7: End force-displacement graphs with principal path in black and first bifurcated branch in orange. Empty square marks represent the location of the bifurcation points. In transparent plain orange line is displayed the results on the discrete model for comparison. (a) Results using the micromorphic equivalent medium. (b) Results using the strain-gradient model. (c) values of deformation and deformation shift for the micromorphic model at the output point and comparison with discrete results at the same point.

reach the almost entire length of the system **??**. The predicted long-wavelength instability followed by a localization is thus confirmed. Author would like to emphasize that the more springs are present in the system, the smaller are the amplitudes of the observed oscillations but this amplitude also depends on the system's stiffness parameters (K_i, M_i, N_i $i = 1, 2$). This oscillating feature has been observed also experimentally and numerically in the literature [18, 19].The localization starts at one end of the system due to imperfect boundary conditions that break the periodicity.

When using the micromorphic equivalent medium, the principal path is appropriately captured and the limit point corresponds to point $(\Delta_E, F) = (0.525731, 0.9711376579)$ with relative error of the order of magnitude of the computer's accuracy on both displacement and force values. Figure 9a presents the End force-displacement curve for the micromorphic equivalent medium. No bifurcation point is detected after the limit point using a perfect system. As a consequence the localization phenomenon cannot

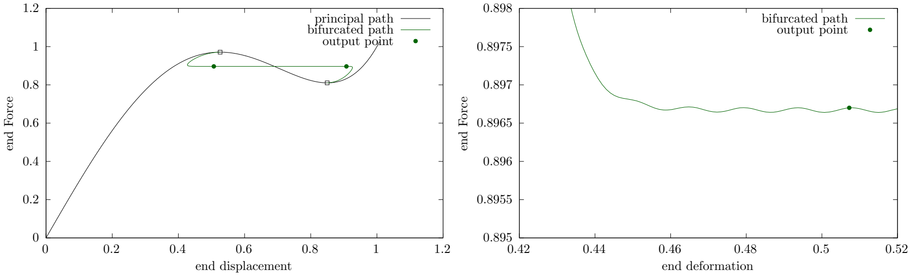

(a) (b) zoom

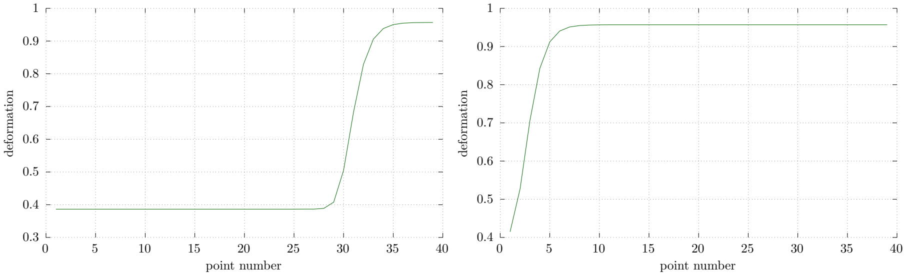

(c) output point 1 (d) output point 2

Fig. 8: Numerical results of computation on the discrete system. (a) End force-displacement graph with principal path in black and first bifurcated branch in green. Empty squares mark the location of bifurcation points and the plain circles the computation points for which bifurcated modes are outputted. (b) and (c) bifurcation modes represented in terms of deformation corresponding to the plain circle output points.

be captured this way. Using an imperfection of 0.1% on the stiffness of the first element, the beginning of the discrete bifurcation branch is captured but the plateau cannot be reached. Additionally, no bifurcation point can be identified because of imperfection. The point where the imperfect curve diverges from the perfect one happens $(\Delta_E, F) = (0.511623, 0.9704268022)$, with relative error of $2.7\ .10^{-2}$ on the displacement and 7.10^{-4} on the force value. Modifying the imperfection amplitude leads to a modification of the "bifurcation point" whereas changing the number of elements in the computation implies a change in the proximity of the branch to the principal path. As so, a higher number of elements leads to a branch closer to the principal path and a larger imperfection leads to an increasing value for the bifurcation point displacement force value. If one plots the value of the deformation and deformation shift across the elements (cf Figure 9c), the localized mode does not appear. The micromorphic medium seems to lack, in essence, the ability to appropriately capture localization as it can capture the onset, if imperfections are introduced, but cannot reproduce the Maxwell line.

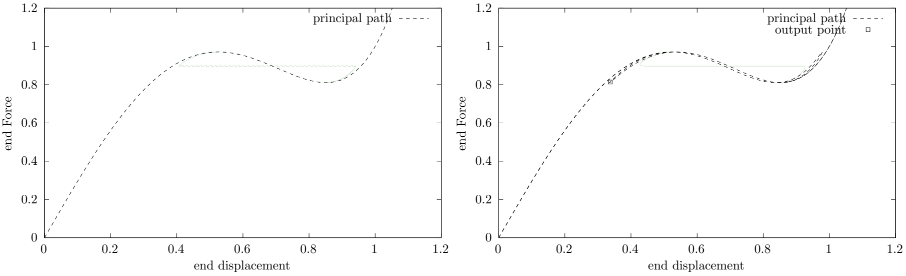

(a) no imperfection

(b) with imperfection

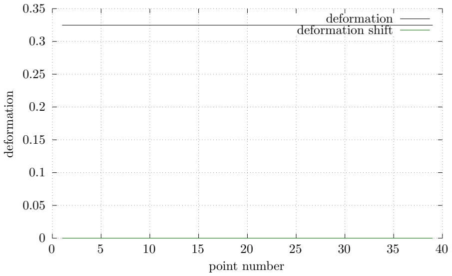

(c) micromorphic deformation mode

Fig. 9: End force-displacement graphs for computations using the micromorphic equivalent medium. (a) perfect model, (b) imperfection of 0.1% in the model on the stiffness of first element. (c) values of deformation and deformation shift for the micromorphic model at the output points

When using the strain-gradient equivalent medium, the principal path is appropriately captured with a limit point located at $(\Delta_E, F) = (0.525731, 0.9711376579)$ with relative error of the order of magnitude of the computer's accuracy on both displacement and force values. Right after this limit point, a bifurcation point is detected at point $(\Delta_E, F) = (0.5262165, 0.9711368274)$ with relative error of 7.10^{-4} on the displacement and of the order of magnitude of the computer's accuracy on the force value. The subsequent bifurcating branch seems to be in very good agreement with the reference discrete branch but does not display any oscillations (cf. Figure 10b). The associated deformation mode corresponds to a localization propagating along the system's length with values agreeing with those of the discrete model. It can thus be concluded that the strain gradient model is able to capture in a satisfactory manner the localization behavior and reproduces accurately the Maxwell line but not the oscillations appearing along this line.

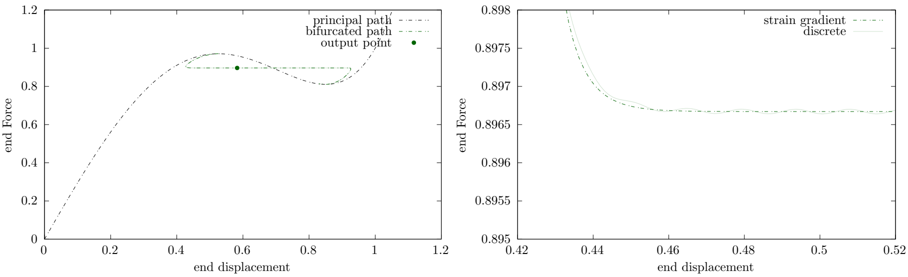

(a)

(b) zoom

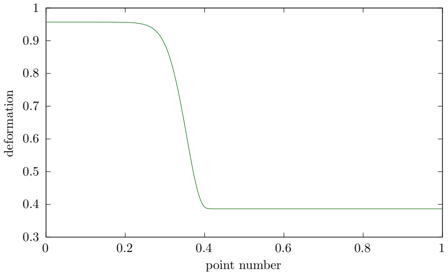

(c) strain-gradient deformation mode

Fig. 10: End force-displacement graphs for computations using the strain-gradient equivalent medium. (a) perfect model, (b) imperfection of 0.1% in the model on the stiffness of first element. (c) values of deformation and deformation shift for the micromorphic model at the output points

From this second numerical study of a long-wavelength bifurcating system, it appears that both models are able to capture de limit point accuratelry but only the strain-gradient model can capture the bifurcation point and subsequent localization that appear afterwards. An imperfect micromorphic model has been proposed to try to capture the bifurcated branch. This model could propose an equilibrium path that is different from the perfect principal path but this path does not corresponds to the discrete bifurcated branch and especially failed to capture the Maxwell line. This second numerical study is of great importance as it shows the benefits of using strain-gradient equivalent medium when localization phenomena are to be modelled.

Conclusion

The objective of this paper was to question the ability of two families of generalized continua (namely micromorphic of strain-gradient) in capturing appropriately onset and post-bifurcated behavior of systems displaying either a patterning type of bifurcation (meaning short-wavelength instability) or a localization phenomenon following a long-wavelength instability. The studied system is an assembly of non-linear springs attached to direct and next-to-neighbor nodes and with stiffness parameters adjusted to display one or the other type of instability. The equivalent media energy are built analytically by microscopic analysis for the micromorphic medium or by Taylor expansion for the strain-gradient medium. A numerical study has been carried out to compare quantitatively the results with a reference computation on a discrete system. It appears that the micromorphic equivalent medium is the only one able to appropriately capture the onset and the post-bifurcation regime when a short-wavelength instability appears, creating a pattern of deformation, while the strain-gradient equivalent medium is the only one able to appropriately capture the localization phenomenon appearing after a long-wavelength instability.

This study, on a very simple system, allows us to build models analytically and thus avoiding possible errors stemming from numerical approximations. Moreover, the conclusions drawn out in this paper explain the choice made by [10] to use a micromorphic model at the macroscopic scale in their numerical homogenization. Indeed, the objective of their work was to capture the patterning instability that spreads on two unit cells and it appears that this can only be done via micromorphic type models.

Of course, the two types of models compared in this study could be combined and this is the authors recommendation if both localization and patterning are expected to happen in the modelled system. This work is currently under investigation, along with studying the ability of each model to capture non-commensurate instabilities that would appear if mode complex models are at stake, as suggested in [9]

5 Acknowledgements

This work was supported by the Agence Nationale de la Recherche (ANR) Project MAX-OASIS ANR-19-CE08-0005, the Center of Research of Ecoles de Saint-Cyr Coëtquidan (CREC) at the Military Academy of Saint-Cyr Coëtquidan and the Institut de Recherche Dupuy de Lôme at University of Bretagne Sud. The author also would like to thank professors N. Triantafyllidis and S. Neukirch for their advices and fruitful discussions and professor R.S.Elliott for his scientific guidance and help with numerical implementations.

References

[1] Brechet, Y., Embury, J.D.: Architectured materials: Expanding materials space. Scripta Materialia **68**(1), 1–3 (2013). https://doi.org/10.1016/j.scriptamat.2012.07.038. Accessed 2021-08-02

[2] Barthelat, F.: Architectured materials in engineering and biology: fabrication, structure, mechanics and performance. International Materials Reviews **60**(8), 413–430 (2015). https://doi.org/10.1179/1743280415Y.0000000008. Publisher: Taylor & Francis _eprint: https://doi.org/10.1179/1743280415Y.0000000008. Accessed 2021-07-29

[3] Poncelet, M., Somera, A., Morel, C., Jailin, C., Auffray, N.: An experimental evidence of the failure of Cauchy elasticity for the overall modeling of a non-centro-symmetric lattice under static loading. International Journal of Solids and Structures **147**, 223–237 (2018). https://doi.org/10.1016/j.ijsolstr.2018.05.028. Accessed 2021-09-28

[4] Combescure, C., Elliott, R.S., Triantafyllidis, N.: Deformation patterns and their stability in finitely strained circular cell honeycombs. Journal of the Mechanics and Physics of Solids, 103976 (2020)

[5] He, Y., Zhou, Y., Liu, Z., Liew, K.M.: Buckling and pattern transformation of modified periodic lattice structures. Extrem. Mech. Lett. **22**, 112–121 (2018). https://doi.org/10.1016/j.eml.2018.05.011

[6] Papka, S.D., Kyriakides, S.: Biaxial crushing of honeycombs: —part 1: Experiments. International Journal of Solids and Structures **36**(29), 4367–4396 (1999)

[7] Auffray, N., Dirrenberger, J., Rosi, G.: A complete description of bi-dimensional anisotropic strain-gradient elasticity. International Journal of Solids and Structures **69**, 195–206 (2015)

[8] Triantafyllidis, N., Bardenhagen, S.: On higher order gradient continuum theories in 1-D nonlinear elasticity. Derivation from and comparison to the corresponding discrete models. J. Elast. **33**(3), 259–293 (1993). https://doi.org/10.1007/BF00043251

[9] Truskinovsky, L., Vainchtein, A.: Quasicontinuum modelling of short-wave instabilities in crystal lattices. Philos. Mag. **85**(33-35), 4055–4065 (2005). https://doi.org/10.1080/14786430500363270

[10] Rokoš, O., Ameen, M.M., Peerlings, R.H.J., Geers, M.G.D.: Micromorphic computational homogenization for mechanical metamaterials with patterning fluctuation fields. J. Mech. Phys. Solids **123**, 119–137 (2019) https://arxiv.org/abs/1810.11069. https://doi.org/10.1016/j.jmps.2018.08.019

[11] Combescure, C., Henry, P., Elliott, R.S.: Post-bifurcation and stability of a finitely strained hexagonal honeycomb subjected to equi-biaxial in-plane loading. International Journal of Solids and Structures **88**, 296–318 (2016)

[12] Combescure, C., Elliott, R.S.: Hierarchical honeycomb material design and optimization: Beyond linearized behavior. International Journal of Solids and Structures **115**, 161–169 (2017)

[13] Eriksen, J.L.: Phase Transformations and Material Instabilities in Solids. Elsevier, ??? (2012)

[14] Elliott, R.S., Shaw, J.A., Triantafyllidis, N.: Stability of thermally-induced martensitic transformations in bi-atomic crystals. J. Mech. Phys. Solids **50**(11), 2463–2493 (2002). https://doi.org/10.1016/S0022-5096(02)00012-1

[15] Elliott, R.S.: Multiscale bifurcation and stability of multilattices. J. Comput. Mater. Des. **14**(SUPPL. 1), 143–157 (2007). https://doi.org/10.1007/s10820-007-9075-8

[16] Doedel, E.J., Champneys, A.R., Dercole, F., Fairgrieve, T.F., Kuznetsov, Y.A., Oldeman, B., Paffenroth, R., Sandstede, B., Wang, X., Zhang, C.: Auto-07p: Continuation and bifurcation software for ordinary differential equations (2007)

[17] Le, K.: Introduction to micromechanics: Classical and quantum mechanics. Nova Science, New York (2011)

[18] Forest, S., Blazy, J.S., Chastel, Y., Moussy, F.: Continuum modeling of strain localization phenomena in metallic foams. J. Mater. Sci. **40**(22), 5903–5910 (2005). https://doi.org/10.1007/s10853-005-5041-6

[19] Findeisen, C., Forest, S., Hohe, J., Gumbsch, P.: Discrete and continuum modelling of size effects in architectured unstable metamaterials. Contin. Mech. Thermodyn. **32**(6), 1629–1645 (2020). https://doi.org/10.1007/s00161-020-00870-8